AN IMPROVED CORRELATION FOR TURBINE ENDWALL LOSS

John D. Coull*

University of Oxford, Oxford, UK

ABSTRACT

To develop high performance turbomachinery, we need accurate preliminary design correlations to guide us towards optimal system and component configurations. Endwall (or secondary) loss has a significant impact on turbine efficiency, but it remains challenging to predict. Most existing correlations are based on well-conditioned linear cascade experiments, but these generally rely on limited databases and do not include the effect of turbine-realistic inlet conditions, which can increase loss significantly.

This paper develops a new correlation to help address these deficiencies. The new method is physics-based and tuned to a large database of linear cascade computations with varying inlet conditions. Endwall loss is decomposed into Wetted Area Loss and Secondary Flow Loss. The Wetted Area Loss represents dissipation in the endwall boundary layers, in a similar manner to the approach of Denton [1]. The Secondary Flow Loss correlates with the secondary vorticity predicted by classical theory, e.g. Hawthorne [2], and is strongly dependent on the thickness and shape of the incoming endwall boundary layer.

Validation with literature cascade experiments shows that the new correlation reduces the average error by >30% compared to the best existing method, which was fit to these data, and more accurately predicts sensitivity to design parameters. The new method predicts a realistic increase in loss when moving from cascade to turbine-like inlet conditions, and thus helps to reconcile the historical mismatch between endwall losses in cascades and real turbines.

1. INTRODUCTION

Accurate preliminary design representations are essential to develop successful turbomachinery: simple mean-line and throughflow models can be rapidly iterated to guide a system towards an optimal configuration. These methods rely on correlations for aerodynamic loss, which must have: (1) absolute accuracy, to predict the performance of the new machine; and (2) have the correct sensitivity to design parameters, in order that the correct optimum is found. In this way, the preliminary design sets the overall design requirements for each component. Significant effort is then expended on detailed component design to optimize performance, e.g. using Computational Fluid Dynamics (CFD), optimization, experimental data and prior experience. Nonetheless, the resultant machine efficiency is still largely determined by preliminary design decisions.

For axial turbines, the flow around the blade endwalls is typically responsible for a third of the lost efficiency [1]. This endwall loss component has proven hard to correlate, as it is dependent on multiple physical processes and is sensitive to the details of the flow entering the blade row.

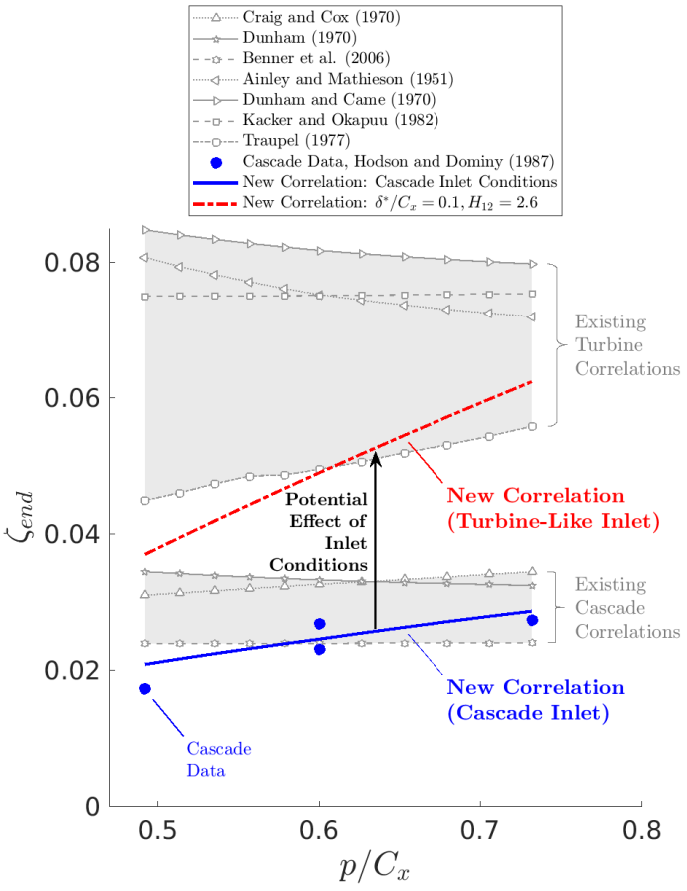

FIGURE 1: Closing the gap between cascades and engines: the new correlation can account for more realistic inlet conditions. Experimental data from [3] [4], showing the effect of varying pitch.

*Corresponding author: john.coull@eng.ox.ac.uk

1.1 Endwall Loss Mechanisms

Our understanding of endwall loss is largely built on simplified linear cascade models, which replicate much of the physics of real turbines. One key feature of the endwall flow is the "secondary flows". The incoming boundary layer rolls up into Horse-Shoe Vortices upstream of the leading edges, and the vorticity is re-orientated and stretched, generating a streamwise vorticity component at the blade row exit [5]. The rotational energy of the resultant secondary vortices can generate significant loss due to mixing. The strength of these vortices increases with flow turning and decreases with outlet-to-inlet velocity ratio, and is strongly affected by the thickness and shape of the inlet boundary layer [6]. Detailed descriptions of secondary flow structures are given in the reviews of Sieverding [7] and Langston [8]. In addition to the secondary flows, significant loss is generated by the boundary layers on the endwall platforms, in particular in high velocity regions, [6] [9].

In real turbines, there are additional factors affecting endwall loss which are generally not present in cascades. First, the geometry is more complex. Platforms have gaps and seals between components, and often sealing flows. All turbines blades are three-dimensional by nature due to radial flow variation and intentional detailed design features such as lean and sweep. Second, the flow field at the inlet to each blade row can be unsteady and spatially complex: the secondary flows from one blade row generate a complex vorticity field which convects into subsequent blade rows, tending to increase the endwall losses. In contrast, almost all linear cascade testing has been performed with relatively thin, turbulent colinear boundary layers. One motivation of the current work is to better account for this mismatch between cascade and turbine inlet conditions.

1.2 Existing Correlations: Turbines vs. Cascades

Historically, there have been two approaches to developing useful preliminary design correlations for endwall loss:

1. **Cascade-Based Correlations.** Using large datasets of linear cascade tests, this approach has the advantage of: (a) enabling accurate separation of profile and endwall losses; (b) enabling relatively large sets of blade designs to be tested; and (c) enabling some of the physical processes to be captured. The main problem with these methods is that they tend to under-predict endwall loss in real turbines, which limits their usefulness.
2. **Turbine-Based Correlations.** Measurements of overall turbine efficiency can be correlated by simultaneously fitting all components of loss (Endwall, Profile and Over-Tip Leakage Loss). Without accurate breakdown of loss components there is greater uncertainty in the endwall loss obtained with this approach. Turbine rigs are also much more complex than linear cascades, so the fitting datasets are smaller. This issue may be partly mitigated by using a form of correlation based on linear cascade tests, then re-tuning the coefficients for turbines (e.g. [10]). These re-tuned methods may predict reasonable levels of loss for real turbines, but do not explicitly account for the physical effects, noted above, that cause higher loss in turbines compared to cascades.

Figure 1 compares the predictions of several methods that use these approaches. The variation of net endwall loss with pitch-to-axial-chord ratio (p/C_x) are shown, for the cascade data of Hodson and Dominy [3], [4]. Three existing methods based on cascade data are shown:

- Craig and Cox [11] correlated endwall loss with aspect ratio, velocity ratio and a blade lift parameter.
- Dunham [12] correlated endwall loss with aspect ratio, flow angles and inlet boundary layer thickness.
- Benner et al. [13] fitted an empirical correlation for net endwall loss to a range of cascade data from the literature.

As shown in Fig. 1, these method give a similar level of loss as the experiments, though only the Craig and Cox method correctly captures the trend of increasing endwall loss with increasing pitch. The Benner method is the most accurate of the three, perhaps unsurprisingly given that the Hodson and Dominy data was included in their fitting database. It is notable that none of these methods account for the shape factor of the inlet boundary layer, H_{12}, which has historically been typically constant (~1.4) for almost all cascade tests. As noted by Coull and Clark [14], inlet shape factors in turbines will tend to be higher, in part because of the change of reference frame between blade rows.

Four methods tuned to overall turbine efficiency are included in Fig. 1:

- Ainley and Mathieson [15] correlated endwall loss with an external-style lift coefficient, based on an analogy with wing tip vortices.
- Dunham and Came [10] re-tuned the cascade correlation of Dunham [12] to better fit overall turbine efficiency. This re-tuning for turbines typically multiplies endwall loss by ~2.5 compared to Dunham's cascade method.
- Kacker and Okapuu [16] modified Dunham and Came's model to reduce the endwall loss for low aspect ratio blades.
- Traupel [17] developed the form of his correlation using cascade data, and then re-tuned it to better match available turbine data.

These correlations all predict higher loss than the cascade experiments, as one would expect. However it is unclear from this comparison which method may be the most accurate for an equivalent turbine. There is significant variation between the methods, of around 60%, suggesting very high uncertainty. Only the method of Traupel predicts the increase in loss with pitch/chord that was noted in the cascade data.

1.3 Paper Aim: Closing the Gap between Cascades and Turbines

It is clear from Fig. 1 that there is a disconnect between the cascade-based and turbine-based methods, with very little understanding of why endwall loss is higher in turbines. This paper aims to develop a new correlation that can better reconcile the predictions of cascade and turbine endwall loss. The new correlation accounts for both inlet boundary layer thickness *and* shape factor. Using the inlet boundary layer parameters measured in the cascade tests, the blue line in Fig. 1 yields an accurate prediction

of the data. The red line shows an example of a more turbine-realistic prediction, obtained by setting a thicker inlet boundary layer ($\delta^*/C_x = 0.1$) and higher shape factor ($H_{12} = 2.6$). This shift of inlet conditions effectively multiples the cascade loss by $1.8 \rightarrow 2.3$. This prediction is close to the turbine-based method of Traupel, and suggests that much of the difference between cascade and turbine endwall loss is caused by the inlet conditions.

The key features of the new correlation are:

1. It explicitly models the loss caused by endwall boundary layer dissipation and secondary-flow-induced loss, [6].
2. It relies largely on analytical models to minimize the number of empirical tuning coefficients.
3. It captures the effect of inlet boundary layer thickness and shape factor, using classical secondary flow theory [14].
4. Coefficient tuning is performed using a large database of cascade CFD cases.
5. Blind validation is performed with experimental cascade data from the literature. The new method achieves greater accuracy than existing methods, and is better able to predict the observed experimental trends.

1.4 Paper Outline

The paper is arranged as follows: §2 outlines the correlation formulation; §3 describes the tuning process with the CFD database; and §4 compares the predictions to experimental data. A brief discussion of the implications and remaining challenges is given in §5.

2. CORRELATION FORMULATION

The net kinetic energy loss through a cascade, ζ_{total}, may be written as:

$$\zeta_{total} = \frac{\overline{V_{2-is}^2} - V_{2-mix}^2}{\overline{V_{2-is}^2}} \tag{1}$$

where $\overline{V_{2-is}^2}$ is the mass-averaged square of isentropic exit velocity, calculated from the inlet total and exit static conditions, and V_{2-mix} is the mixed-out exit flow velocity. Assuming zero tip clearance, the Net Endwall Loss ζ_{end} is calculated as:

$$\zeta_{end} = \zeta_{total} - \zeta_{profile} \tag{2}$$

In general, the profile loss $\zeta_{profile}$ can be taken as the midspan loss provided that the cascade aspect ratio is sufficiently high.

2.1 Input Parameters

The correlation relies only on preliminary design parameters, so no detailed information about the blade sections or loading style is used. Taking the axial chord C_x as the reference length, the overall formulation may be written as:

$$\zeta_{end} = f\Bigg(\underbrace{\alpha_1, \alpha_2, \frac{V_1}{V_2}, \frac{\rho_1}{\rho_2}}_{\text{mainstream flow}}, \underbrace{\frac{\delta^*}{C_x}, H_{12}}_{\text{inlet endwall boundary layer}}, \underbrace{\frac{p}{C_x}, \frac{h}{C_x}, \frac{T_{max}}{C_x}}_{\text{blade geometry}}, \underbrace{\frac{X_{US}}{C_x}, \frac{X_{DS}}{C_x}}_{\text{platform lengths}} \Bigg) \tag{3}$$

The mainstream flow is captured by the inlet and exit angles (α_1, α_2), and the velocity ratio (V_1/V_2). The density ratio (ρ_1/ρ_2) has only a limited influence. The inlet boundary layer is characterized by the displacement thickness (δ^*) and shape factor (H_{12}). Blade geometry is described by axial chord (C_x), pitch (p), span (h) and section maximum thickness (T_{max}); this latter parameter has a relatively weak influence. The final parameters are the axial lengths of the upstream (X_{US}) and downstream (X_{DS}) endwalls. These distances set the distances of the inlet and outlet accounting planes from the leading and trailing edge respectively. The correlation makes no *explicit* account of Mach or Reynolds number. Marsh [18] showed theoretically that Mach number has a relatively weak impact on secondary flows for turbines, while several results show only a weak dependence on Reynolds number (e.g. [4], [19]).

The endwall loss is correlated as the sum of Wetted Area Loss ζ_{wet} and Secondary-Flow-Induced Loss ζ_{sec}:

$$\zeta_{end} = \zeta_{wet} + \zeta_{sec} \tag{4}$$

These components are described in the following sections.

2.2 Wetted Area Loss ζ_{wet}

From Denton [1], the entropy generation rate $\dot{S}$ in the endwall boundary layer can be expressed by the integral:

$$\dot{S} = \int C_D \frac{\rho V^3}{T} dA \tag{5}$$

where the density ρ, velocity V and temperature T are the freestream values. The wetted area loss is calculated as the sum of three zones on the platform (upstream, in-passage and downstream), so that:

$$\zeta_{wet} = \zeta_{US} + \zeta_{pass} + \zeta_{DS} \tag{6}$$

The upstream and downstream terms are calculated directly from the dissipation generation rate in Eq. (5), assuming that the velocities are equal to the inlet and exit values respectively:

$$\zeta_{US} = 4C_D \left(\frac{C_x}{h \cos \alpha_2} \right) \left(\frac{V_1}{V_2} \right)^3 \left(\frac{X_{US}}{C_x} \right) \tag{7}$$

$$\zeta_{DS} = 4C_D \left(\frac{C_x}{h \cos \alpha_2} \right) \left(\frac{X_{DS}}{C_x} \right) \tag{8}$$

It is harder to define an "average" velocity and area for the in-passage loss. By examining integrated values of isentropic $\rho V^3/T$ from the CFD for around 200 cascades, it was found that this term can be reasonably approximated by the simple expression:

$$\zeta_{pass} = 4.363 \; C_D \left(\frac{C_x}{h} \right) \tag{9}$$

Equation (9) is accurate to around 10-15% (95% confidence), which introduces only a small error in the total endwall loss. Thus the total wetted area loss is given by:

$$\zeta_{wet} = C_D \left(\frac{C_x}{h} \right) \left(\frac{4}{\cos \alpha_2} \left[\left(\frac{V_1}{V_2} \right)^3 \left(\frac{X_{US}}{C_x} \right) + \left(\frac{X_{DS}}{C_x} \right) \right] + 4.363 \right) \tag{10}$$

In line with [6], a dissipation coefficient of $C_D = 0.002$ is assumed, which is a reasonable approximation for many turbomachinery flows [1]. Note that for non-parallel endwalls, surface lengths should be used in lieu of axial lengths.

2.3 Secondary-Flow-Induced Loss

The Secondary-Flow-Induced Loss ζ_{sec} takes the form:

$$\zeta_{sec} = \zeta_{sec-mix} + \zeta_{SKE} \tag{11}$$

The two terms represent the Secondary-Flow-Induced-Mixing loss and the Secondary Kinetic Energy (SKE) respectively. This separation is based on the analysis of Coull et al. [20].

2.3.1 Secondary-Flow-Induced-Mixing Loss $\zeta_{sec-mix}$. When the inlet boundary layer is thin ($\delta^* \rightarrow 0$), the SKE is low but there are still significant mixing losses generated by the secondary flows. In line with the findings of Coull [6], $\zeta_{sec-mix}$ is approximately proportional to the non-dimensional passage vortex circulation:

$$\zeta_{sec-mix} = 2\left(\frac{p\cos\alpha_2}{h}\right)\left(0.01442\,\Gamma^*_{sec}\right) \tag{12}$$

The factor 2 represents contributions from both endwalls. This term is inversely proportional to an aspect ratio ($h/p\cos\alpha_2$), which is approximately equal to the inverse of span-to-throat used by Craig and Cox [11]. The coefficient (0.01442) in Eq. (12) is empirical and has been tuned to the computational cascade database, as described in §3. The non-dimensional Passage Vortex Circulation, Γ^*_{sec}, is calculated from secondary flow theory using the method of [14]. In this form, it is independent of the inlet conditions and aspect ratio, and is a function of the midspan (2D section) design only:

$$\Gamma^*_{sec} = V^*\frac{\Delta T^* C_x}{p\cos\alpha_2} + \left|\frac{V_1}{V_2}\frac{\sin\alpha_1}{\cos\alpha_2} - V^*\tan\alpha_2\right| \tag{13}$$

where:

$$V^* = \left(1 - \sqrt{1-(V_1/V_2)^2}\right) \tag{14}$$

Equation (13) shows that secondary flows increase in strength with increasing flow turning, velocity ratio V_1/V_2 and ΔT^*, which is the non-dimensional difference in transit time between flow passing over the pressure and suction surfaces of the blade.

2.3.2 Transit Time Difference ΔT^*. If the blade geometry and loading distribution are known, ΔT^* can be calculated by integrating the inverse velocity around the surface, [6]:

$$\Delta T^* = \oint\left(\frac{V_2}{V}\right)d\left(\frac{S}{C_x}\right) \tag{15}$$

where V is the boundary layer edge velocity. However, a requirement to know the section geometry and aerodynamic loading is unsatisfactory for preliminary design, which relies on meanline or throughflow representations of the turbine. The transit time is therefore correlated using a subset of the input parameters from Eq. (3):

$$\Delta T^* = f\left(\alpha_1, \alpha_2, \frac{\rho_1}{\rho_2}, \frac{p}{C_x}, \frac{T_{max}}{C_x}\right) \tag{16}$$

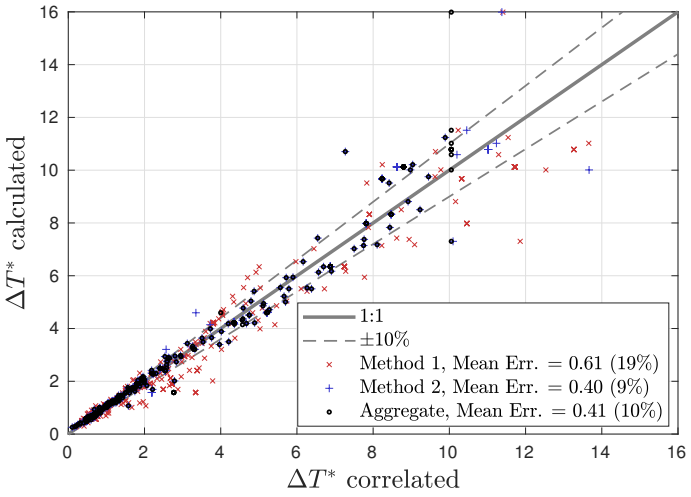

FIGURE 2: Aggregate correlation for Transit Time Difference (ΔT^*) compared to values calculated from Mises for 200 cascades. Details of the methods are given in Appendix A.

The transit time increases as pressure side velocity decreases, which tends to occur for greater turning angles, higher pitch and thinner blades. To fit this correlation, ΔT^* was calculated by applying Eq. (15) to two-dimensional Mises calculations [21] for 200 cascades. The correlation is described in Appendix A. Figure 2 shows that, while there are some outliers, the average fitting error in ΔT^* for the final Aggregate Method is less than 10%.

While satisfactory, the transit time correlation will be a potential source of inaccuracy. In particular, ΔT^* can vary significantly with the detailed blade loading style, which cannot be captured by the input parameters in Eq. (3) and Eq. (16). For example, Pullan et al. [22] found that an aft-loaded profile had lower endwall loss than a fore-loaded design. It may be possible to modify the existing ΔT^* correlation to include additional "design style" input parameters, but this would add significant complexity and likely decrease the robustness of the method.

2.3.3 Secondary Kinetic Energy Loss ζ_{SKE}. "Secondary Kinetic Energy" (SKE) refers to the rotational energy of the secondary flows. Denton [1] argued that some of this energy may be recovered in downstream stages, but in practice most of the SKE will be dissipated within a short distance of the trailing edge (e.g. [20]). As noted above, the current method considers fully mixed-out loss and therefore assumes that all SKE is dissipated.

SKE is heavily dependent on the inlet endwall boundary layer, as demonstrated by Coull and Clark [14]. A thin inlet boundary layer ($\delta^* \rightarrow 0$) tends to generate streamwise secondary vorticity that is concentrated in thin layers near the passage walls. The rotational flow induced by this vorticity is largely canceled out by the mirror vorticity reflected in the passage walls. Therefore the SKE tends to zero, $\zeta_{SKE} \rightarrow 0$, as $\delta^* \rightarrow 0$. Increasing the boundary layer thickness and/or shape factor tends to displace the secondary vorticity away from the walls, reducing mirror cancellation and increasing SKE. These trends can be quantitatively described by classical secondary flow theory, e.g. as described by Hawthorne [23] and Marsh [24].

Using calculations for a large number of cases, [14] showed

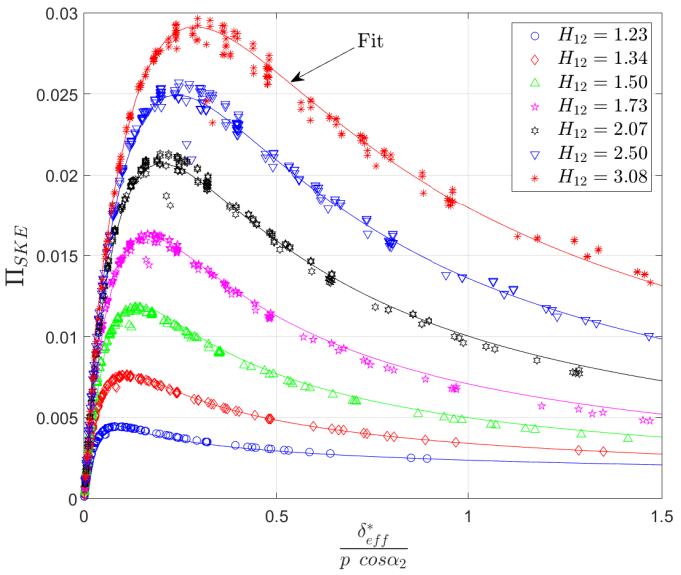

FIGURE 3: Fit for Vorticity Distribution Parameter, Eq. (18). Symbols are numerical calculations from [14].

that numerical SKE calculations using Hawthorne's theory collapse to the following relationship:

$$\zeta_{SKE} = 2\left(\frac{p\cos\alpha_2}{h}\right)\left(\Gamma^*_{sec}\right)^2 \underbrace{\Pi_{SKE}}_{f\left(\frac{\delta^*_{eff}}{p\cos\alpha_2}, H_{12}\right)} \tag{17}$$

where the parameter Π_{SKE} describes how the vorticity distribution in the blade passage affects SKE. The effective displacement thickness δ^*_{eff} is corrected for streamtube contraction effects, as described in the following section. Figure 3 presents the data from [14]. ζ_{SKE} is maximum for high inlet shape factors (H_{12}). As the displacement thickness (δ^*_{eff}) increases, SKE initially rises rapidly before plateauing and reducing. Here, Π_{SKE} is fitted to the numerical results with the following expression, shown on the plot:

$$\Pi_{SKE} = \frac{0.0102\,(H-1)\,D^{\left(\frac{0.170}{H-1}+0.593\right)}}{D^{1.636} + 0.0986\,(H-1) - 0.119} \tag{18}$$

where:

$$H = \max(H_{12}, 1.23) \tag{19}$$

$$D = \frac{\delta^*_{eff}}{p\cos\alpha_2} \tag{20}$$

2.3.4 Correction for Streamtube contraction. The classical theory of Hawthorne ignores any streamtube contraction or twist through the blade row, thus assuming that all fluid remains on two-dimensional planes as it passes through the cascade. This assumption can lead to discrepancies, and therefore a simple correction is made to the displacement thickness.

To demonstrate the issue, the symbols in Fig. 4 show endwall loss values for four cascades from the CFD database, described in detail in §3. The thin lines in these plots show the correlation without any correction for streamtube contraction. Most of the curves show good agreement with the CFD, but a large discrepancy is noted for the highest turning design in Fig. 4(d). For

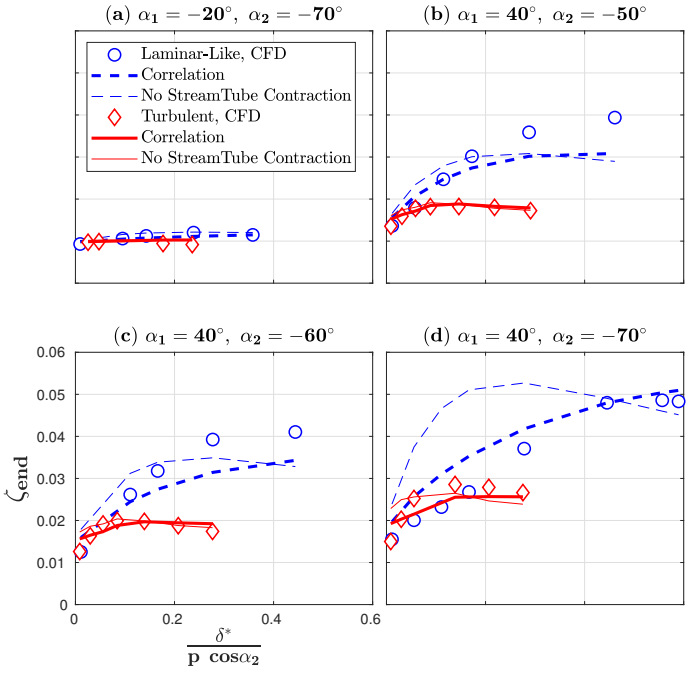

FIGURE 4: CFD and correlation with and without the streamtube contraction correction. Effect of inlet condition for four cascades from [6], Aspect ratio $h/C_x = 3$.

the laminar-like inlet condition, $H_{12} = 2.6$, the theory (thin blue line) predicts a similar peak value of ζ_{end} but under-predicts the boundary layer thickness at which it occurs: $\delta^*/(pcos\alpha_2) \approx 0.2$ compared to ~ 0.6 in the CFD.

The correction reduces the effective δ^*. From the one-dimensional Von Karman momentum integral equation, together with the ratio of exit to inlet flow area ($\cos\alpha_2/\cos\alpha_1$), the following Contraction Factor CF is postulated:

$$CF = (1 + min\,(2.62, H_{12}))\left(\frac{V_2}{V_1} - 1\right)\left(\frac{\cos\alpha_2}{\cos\alpha_1}\right) \tag{21}$$

The shape factor limit (2.62) reflects the maximum value in the CFD database. The CF parameter is limited to be in the range $0 \rightarrow 5$, and the effective inlet displacement thickness is correlated by:

$$\frac{\delta^*_{eff}}{\delta^*} = e^{-0.345CF} \tag{22}$$

The constant (-0.345) has been tuned to the computational cascade database, as described in the following section. The thick lines in Fig. 4 show the corrected correlation, which improves the agreement - especially for the highest turning cascade in Fig. 4(d).

3. TUNING WITH CFD DATABASE

The two empirical coefficients for secondary-flow-induced mixing loss (Eq. (12)) and the streamtube contraction correction (Eq. (22)) were optimized using a database of ~500 CFD cascade calculations with a range of colinear inlet boundary layers.

3.1 Tuning Database

The tuning database includes the cases studied by [6], [26] and [14], alongside additional test cases. Reynolds-Averaged-Navier-Stokes calculations have been performed using the Rolls-Royce HYDRA code [27], on structured meshes with $y^+ \approx 1$ and

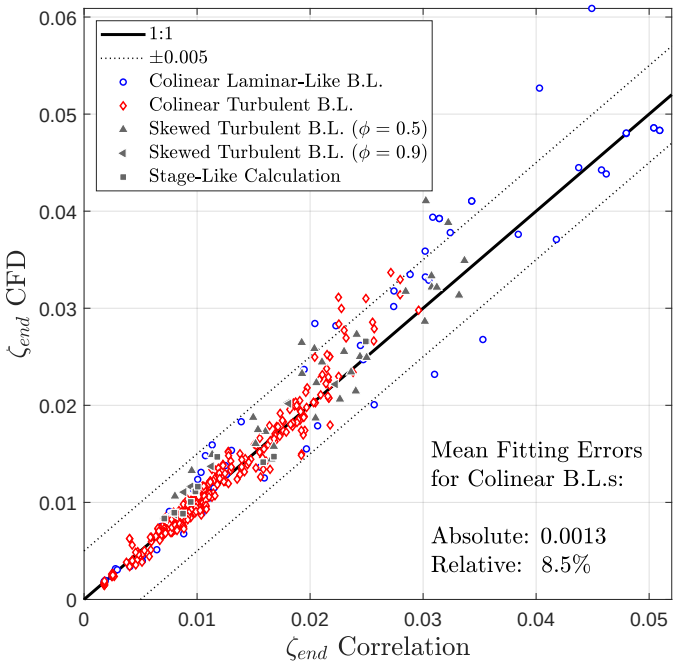

FIGURE 5: Comparison of secondary-flow-induced loss: correlated vs. CFD database.

TABLE 1: Input parameter ranges in CFD database.

Parameter	Symbol	Range
Inlet Angle	α_1	$-20° \rightarrow 40°$
Outlet Angle	α_2	$-70° \rightarrow -50°$
Velocity Ratio	V_1/V_2	$0.265 \rightarrow 0.749$
Inlet Displacement Thickness	δ^*/C_x	$0.003 \rightarrow 0.53$
Inlet Shape Factor	H_{12}	$1.2 \rightarrow 2.62$
Pitch-to-Axial-Chord	p/C_x	$0.573 \rightarrow 2$
Span-to-Axial-Chord	h/C_x	$2 \rightarrow 12$
Blade Maximum Thickness	T_{max}/C_x	$0.15 \rightarrow 0.2$
Upstream Platform Length	X_{US}/C_x	0.8
Downstream Platform Length	X_{DS}/C_x	0.5

around 10 million cells for a single passage. The flow is modeled as fully turbulent using the $k-\omega$ Shear Stress Transport model of Mentor [28]. While higher fidelity simulations may better capture the details of the flow, the current approach gives good accuracy for the prediction of bulk endwall loss [14]. The inlet plane is located $0.8C_x$ upstream of the leading edge, the outlet flow is extracted at a plane $0.5C_x$ downstream of the trailing edge, while the domain exit is a further $0.7C_x$ downstream. Net loss coefficients are calculated by considering constant-area mixing of the outlet flow to a uniform condition [14]. Endwall loss is then defined in the usual manner by subtracting the midspan loss from the passage loss, Eq. (2). Full details of the methods and validation can be found in [14]. The input parameter range for the CFD tuning database is given in Table 1.

3.2 Coefficient Tuning

The two empirical coefficients in Eq. (12) and Eq. (22) were optimized simultaneously to minimize the arithmetic average error in endwall loss coefficient. The resultant fit of ζ_{end} is shown in Fig. 5. Only the cases with colinear inlet boundary layers were used in this training set (red and blue symbols). The average error in loss coefficient is less than 0.0013 (~8.5% relative error). Given the limited degrees of freedom, the fit achieved gives confidence in the method.

3.3 Non-Colinear Inlet Conditions

Additional CFD predictions with more complex inlet conditions were also performed. While not used to tune the correlation, these data are included in Fig. 5 as gray symbols:

- Skew arises due to the change of reference frame between blade rows, and has been shown to enhance secondary flow and endwall loss in turbines, [29]. Skewed boundary layer calculations were included in the current database by mimicking this change in reference for different flow coefficients ($\phi = V_x/U_{blade} = 0.5, 0.9$) at the inlet.
- In a turbine stage, the secondary flows from the stator row convect into the downstream rotor. Here, these inlet conditions are approximated using the outlet flow field from a calculation with a colinear inlet ($\delta^*/C_x = 0.007$, $H_{12} = 1.4$), and accounting for the change of reference frame assuming a 50% reaction turbine.

Inlet boundary layer parameters (δ^*, H_{12}) were calculated for each case by considering only the streamwise (α_1) component of velocity. In general, Fig. 5 shows that these cases are satisfactorily predicted. While encouraging, it is noted that the relatively long inlet duct in the current calculations ($0.8C_x$) is not representative of closely-coupled blade rows. Further work is therefore needed to better understand how such complex inlet conditions affect secondary flows and endwall loss.

4. COMPARISON TO EXPERIMENTS AND PREVIOUS CORRELATIONS

To assess the accuracy of the new method, predictions are now compared to a range of cascade experiments from the litera-

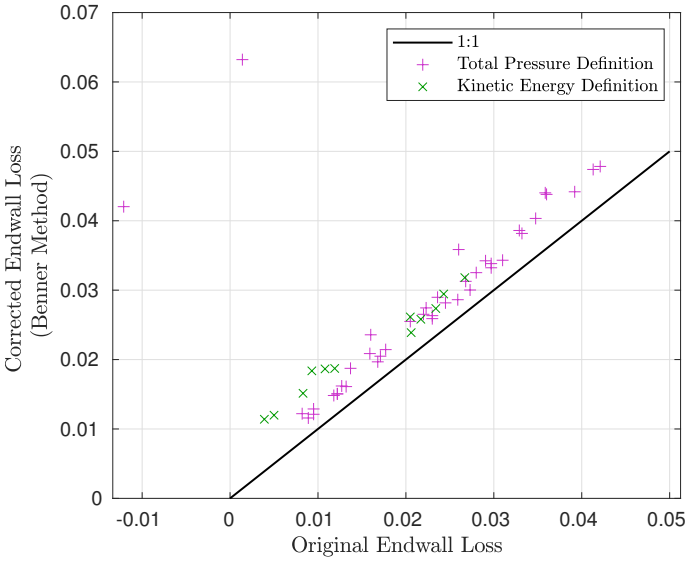

FIGURE 6: The endwall loss correction method of Benner et al. [25] applied to the experimental database.

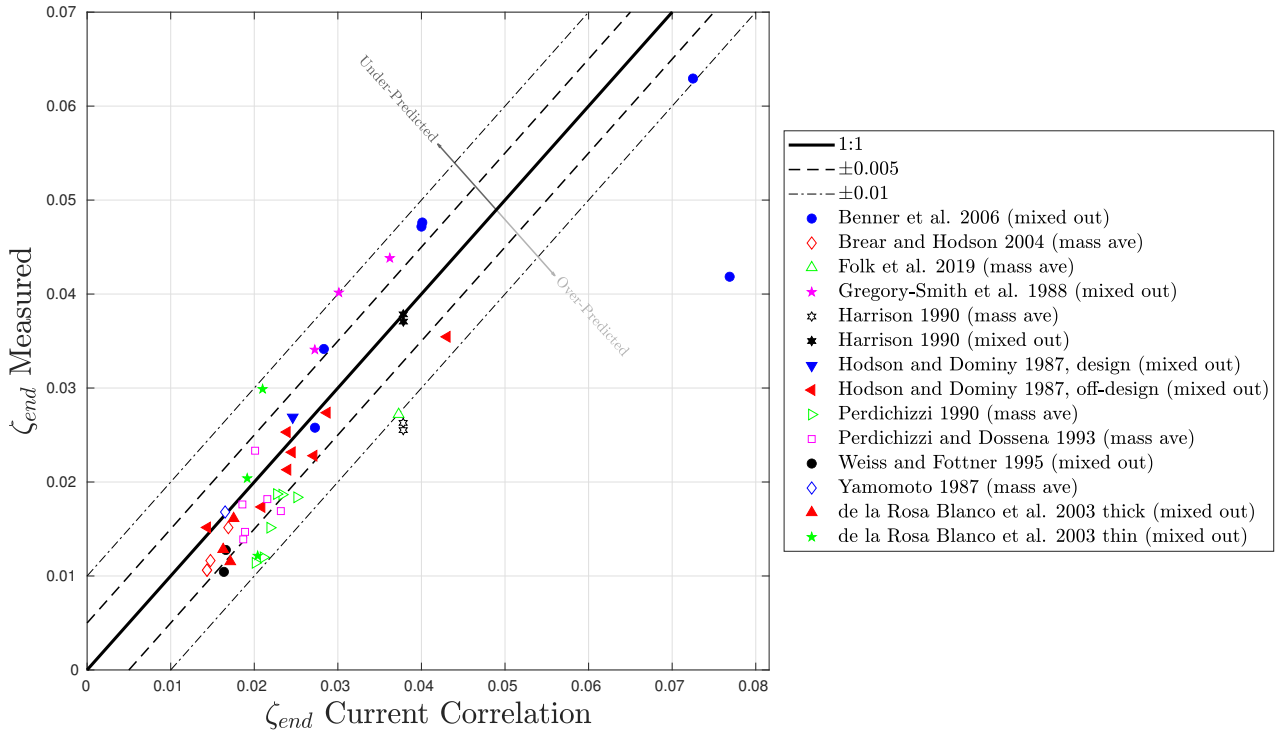

FIGURE 7: Predictions of Current Correlation vs. Measured Net Endwall Loss: filled symbols indicate mixed-out loss; open symbols indicate mass-averaged.

TABLE 2: Mean errors for different correlations (absolute values), ordered by decreasing accuracy.

	Mass-Averaged Cases		Mixed-Out Cases		All Cases	
Method	average	bias	average	bias	average	bias
Current	0.0055	+0.0051	0.0056	+0.0013	0.0055	+0.0029
Benner et al. [13]	0.0120	+0.0120	0.0052	-0.0010	0.0081	+0.0044
Dunham [12]	0.0207	+0.0207	0.0121	+0.0114	0.0157	+0.0153
Craig and Cox [11]	0.0266	+0.0266	0.0140	+0.0081	0.0192	+0.0158
Traupel [17]	0.0265	+0.0265	0.0256	+0.0256	0.0260	+0.0260
Ainley and Mathieson [15]	0.0213	+0.0213	0.0511	+0.0511	0.0387	+0.0387
Kacker and Okapuu [16]	0.0464	+0.0464	0.0546	+0.0546	0.0512	+0.0512
Dunham and Came [10]	0.0512	+0.0512	0.0564	+0.0564	0.0542	+0.0542

ture, summarized in Appendix B. Most of these cases were used by Benner et al. [13] to fit their cascade loss correlation.

4.1 Benner's method for Profile Loss Correction

Typically the two-dimensional (2D) profile loss in Eq. (2) is taken as the midspan loss. However, in many tests the aspect ratio is too low to ensure that the midspan flow is truly two-dimensional. In the first paper of their correlation development, Benner et al. [25] proposed a means to correct the midspan loss to get a better estimate of the "true" profile and endwall breakdown. They showed that this allows a more realistic estimate of endwall loss for a range of cascades. Their approach was to correlate for the spanwise penetration depth of the secondary flow at the blade trailing edge (Z_{TE}). By considering the wetted area ratios, they then use the following scaling factor to relate the midspan loss to the "true 2D" profile loss:

$$\zeta_{profile} \approx \zeta_{mid} \left(1 - \frac{Z_{TE}}{h}\right) \tag{23}$$

where Z_{TE} is the spanwise penetration depth of the secondary flows. Following the approach of Sharma and Butler [30], Benner et al. then correlated Z_{TE}/h with aspect ratio, a modified lift coefficient, the ratio of inlet-to-exit flow areas and the inlet displacement thickness. This approach has been used here to correct all of the reported losses in the cascade database. As shown in Fig. 6, the correction is modest (<0.004) for most cases. The outliers to the top left of the plot are data from Benner et al. [31] at +20° incidence, where the original endwall loss was zero or negative. These cases are therefore particularly sensitive to the accuracy of this correction.

After applying the correction of Benner, all of the reported loss coefficients were converted to kinetic-energy loss referenced

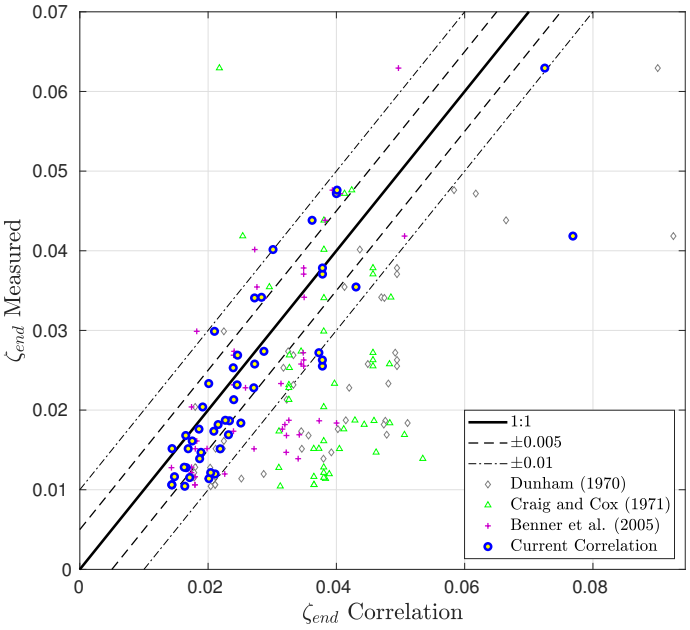

FIGURE 8: Cascade correlations vs. experiments.

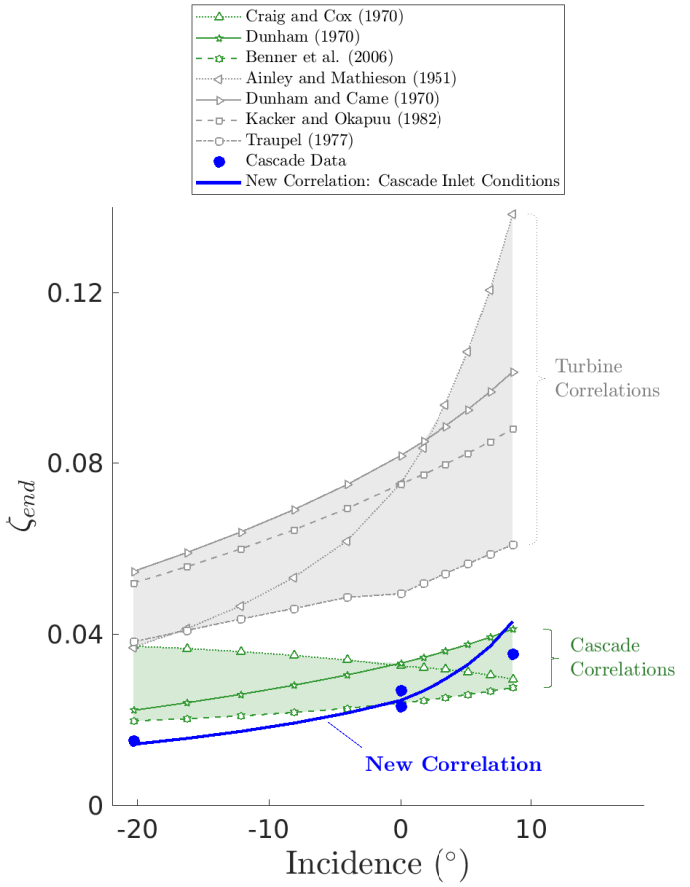

FIGURE 9: Sensitivity to incidence for the data of Hodson and Dominy, [3] [4].

to the outlet conditions (Eq. (1)) and the net endwall loss ζ_{end} calculated (Eq. (2)). Where only gross loss coefficients were given, the loss at the cascade inlet was estimated using the reported inlet boundary layer parameters.

4.2 Predictions vs. Experimental Data

The experiments and new correlation are compared in Fig. 7. The cases are grouped by author and the symbol fill differentiates between mixed-out (filled) and mass-averaged (open) loss definitions. Noting that the correlation was formulated to predict mixed-out loss (see above), mass-averaged data tends to be over-predicted as one would expect, with an average bias for these cases of around +0.005. This bias can be observed in the data of Harrison [32], where both definitions of loss are given: the mass-averaged loss (open black stars) is over-predicted by about 0.011, while the mixed-out loss (filled black stars) is predicted to within ±0.001. All of the cases in Fig. 7 are predicted to within ±0.011 with the exception of one outlier. This outlier is the Benner LS2 blade [25], with very low aspect ratio and +20° incidence. This is the case in Fig. 6 where the original endwall loss was negative. As such there is significant uncertainty in the corrected endwall loss for this data point.

4.3 Accuracy Compared to Other Methods

Table 2 presents the arithmetic average and bias errors for the new correlation and a range of existing methods from the literature, ordered by decreasing accuracy. For the whole dataset, the mean error for the current method (0.0055) is around 30% less than that of Benner et al. (0.0081). Again it is noted that their fitting database included most of these test cases.

In line with Fig. 1, Table 2 shows that the three cascade-based methods (Benner et al., Dunham, Craig and Cox) have the lowest errors. These methods are compared to the data in Fig. 8, and show significantly higher scatter than the new method. As expected, the turbine-based correlations (Traupel, Ainley and Mathieson, Kacker and Okapuu, Dunham and Came) predict significantly higher loss than the cascade values, indicated by the large, positive bias errors in Table 2.

4.4 Parameter Sensitivity

In addition to achieving high absolute accuracy, preliminary design correlations should also predict the sensitivity to key design parameters, so that optimal configurations may be determined. It was noted in Fig. 1 that only the new correlation and those of Craig and Cox [11] and Traupel [17] correctly capture the increase in loss with pitch. To expand on this comparison, Fig 9 shows the variation of net endwall loss with incidence for the Hodson and Dominy cascade, [3] [4]. The data reported were mixed-out losses, again indicated by the filled symbols. Different correlation predictions are overlaid:

- The current correlation gives an accurate replication of the trend and level of loss with varying incidence.
- All of the methods correctly show an increase in loss as incidence increases, with the exception of Craig and Cox [11].
- The cascade correlations of Benner et al. [13] and Dunham [12] also capture the data to a reasonable degree of accuracy.
- The turbine-based correlations all predict higher loss than measured, by a factor of around 2 → 3, but with a similar trend with inlet angle.

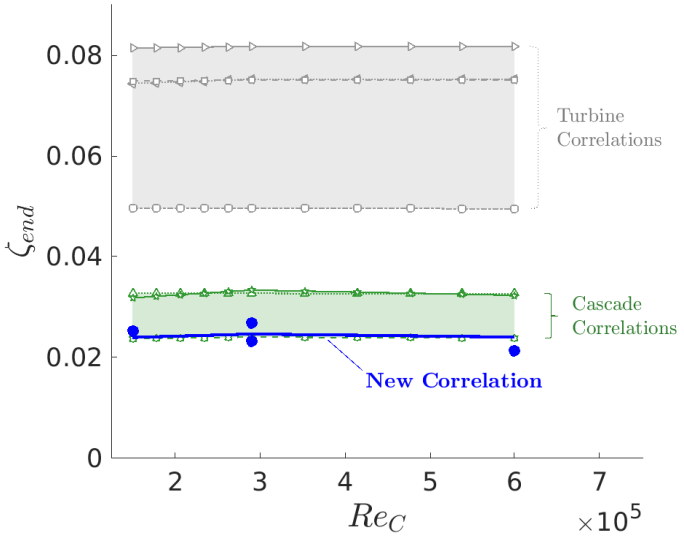

FIGURE 10: Sensitivity to Reynolds number for the data of Hodson and Dominy, [3] [4]. Legend in Fig. 9.

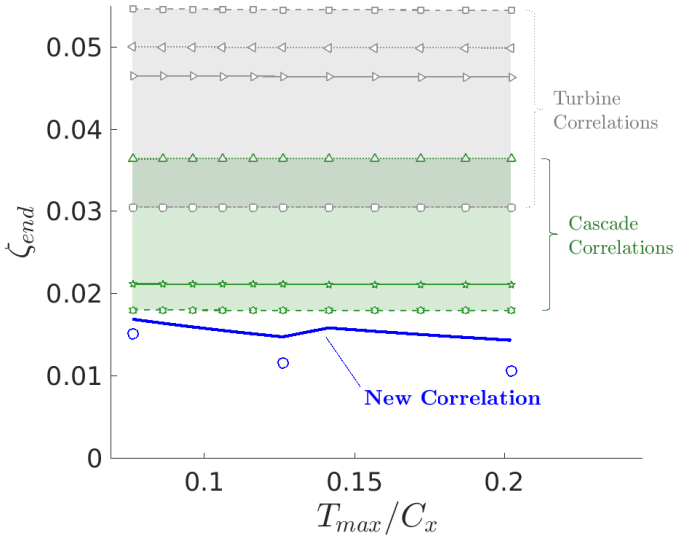

FIGURE 11: Sensitivity to blade thickness, mass-averaged loss coefficients from Brear et al. [33]. Legend in Fig. 9.

Subsequent plots show additional comparisons. In Fig. 10, we observe that Reynolds number had only a modest impact on loss for the Hodson and Dominy cascade. The new correlation is not dependent on Reynolds number, but small variations are predicted due to modest changes in the inlet conditions. A similar insensitivity to Reynolds number has been observed in other cases, e.g. [19].

Figure 11 shows the effect of blade thickness in the data of Brear and Hodson [33]. For the cascades with variable spanwise thickness, the maximum thickness T_{max}/C_x at the endwall has been used as an input parameter. The correlation correctly captures the trend while predicting higher loss than the mass-averaged experimental data, as expected. A small, undesirable, kink in the predictions is evident between $T_{max}/C_x = 1.3 \rightarrow 1.4$, which is caused by a switch between methods for predicting ΔT^*, see Eq. (36). No other method has any sensitivity to thickness.

The effect of inlet displacement thickness is shown for four cascades. Figures 12 and 13 respectively show the thick and thin blades studied by de la Rosa Blanco et al. [34]. The correlation is sensitive to blade maximum thickness T_{max}, and correctly predicts the trend of higher loss for the thin blade. For both blades, the correlation captures the increase in loss with increasing δ^*. However the rise in loss is under-predicted for the thin blade, which likely reflects the complex interaction between the secondary flow and the pressure side separation present for this blade [34]. Figure 14 shows data for Hodson and Dominy [3] [4]. With increasing δ^*, the data show a modest reduction in loss, compared to a modest rise for the correlation; nonetheless the errors remain relatively small. Finally, Fig. 15 shows data for the Durham cascade, [35]. As seen in the experimental data, the correlation predicts a kink at low δ^*, which is caused by variation in the inlet shape factor. In order of increasing δ^*, H_{12} for the three points varied from $1.28 \rightarrow 1.22 \rightarrow 1.42$.

These comparisons demonstrate that the new correlation captures the effects of key parameters more accurately than the existing methods, while demonstrating that the new correlation has better absolute accuracy.

5. DISCUSSION

5.1 The Need for Further Data

It is clear that the new method is more accurate than the previous correlations. There remain, however, several key predictions that remain untested by the available experimental data. Shape factors are likely to be high in turbines [14], but the cascade literature almost exclusively focuses on turbulent inlet profiles with $H_{12} \approx 1.4$. There is therefore a need for systematic experimental studies of cascades with varying inlet shape factor and boundary layer thickness, and more complex inflow conditions as experienced by installed turbines (e.g. §3.3). Such data would enable a more thorough test of the new method, for both accuracy and sensitivity, and highlight gaps in our understanding.

5.2 Application in Turbine Preliminary Design

As Fig. 14 shows, the new method can predict a realistic increase in loss as we move from typical cascade inlet conditions (thin boundary layer, low shape factor) to more representative turbine inlet conditions (thick boundary layer, higher shape factor). Building on this encouraging result, we need to explore how best to apply the method for turbine preliminary design and to formally assess its accuracy:

- The correlated endwall loss is sensitive to the choice of row inlet conditions (δ^* and H_{12}). In practice, these are case-dependent, being affected by upstream components and leakage/sealing flows. Further work is therefore needed to better characterize the variations of inlet conditions and to capture their influence during preliminary design.
- As noted in §1.2, the endwall loss component cannot be accurately determined from turbine test data. However, the accuracy of the method should ultimately be assessed as part of a wider preliminary design prediction, including models of Profile and Over-Tip Leakage Loss.

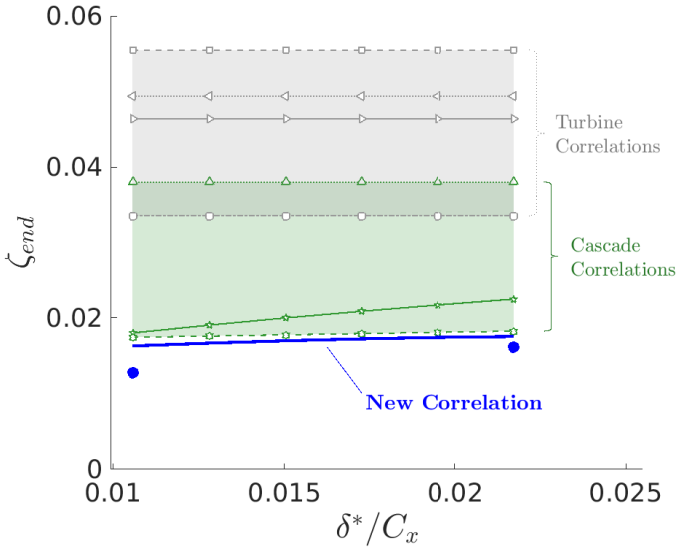

FIGURE 12: Sensitivity to inlet displacement thickness. Mixed-out loss coefficients from de la Rosa Blanco et al. [34], Thick Blade. Legend in Fig. 9.

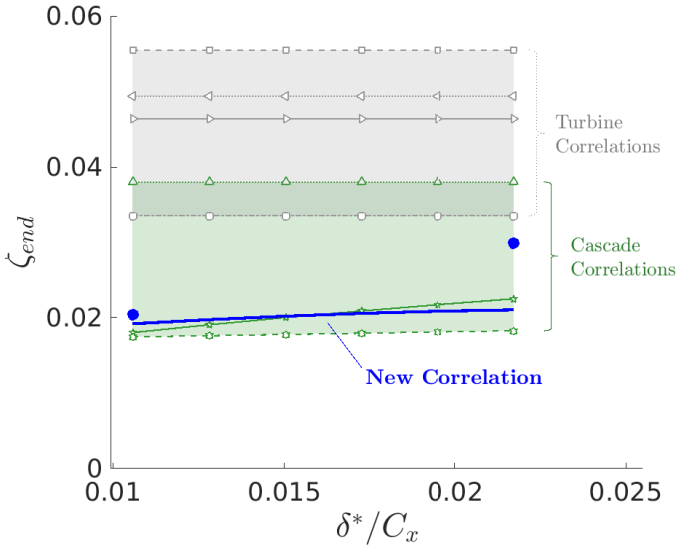

FIGURE 13: Sensitivity to inlet displacement thickness. Mixed-out loss coefficients from de la Rosa Blanco et al. [34], Thin Blade. Legend in Fig. 9.

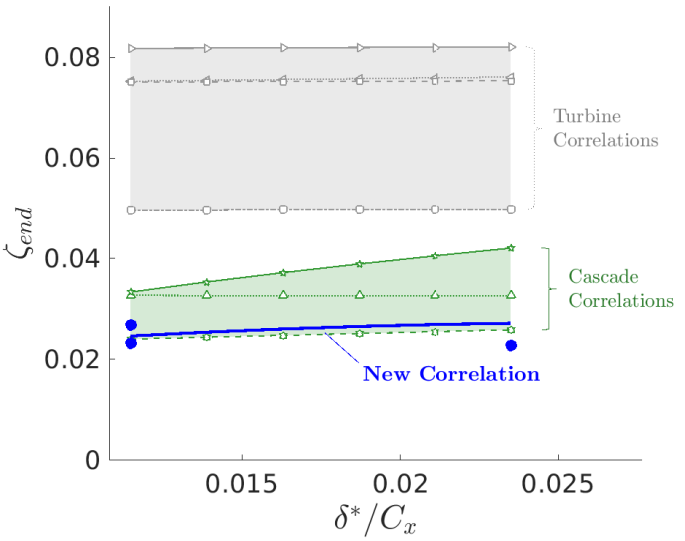

FIGURE 14: Sensitivity to inlet displacement thickness. Mixed-out loss coefficients from Hodson and Dominy, [3] [4]. Legend in Fig. 13.

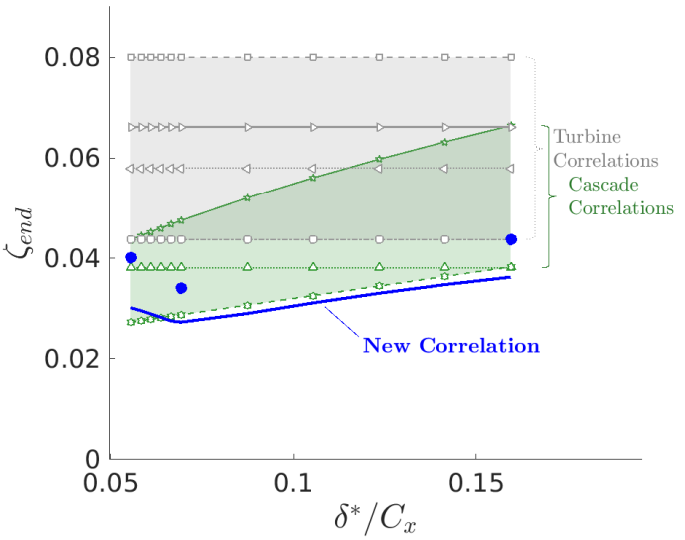

FIGURE 15: Sensitivity to inlet displacement thickness: mixed-out loss coefficients from [35]. Legend in Fig. 9. The kink is caused by variation in inlet shape factor between the cases.

5.3 Potential Improvements to the Method

A key area for potential improvement to the method is the estimate of transit time difference ΔT^* (Appendix A). The current method achieves a satisfactory fit, but a more comprehensive and physical approach would be desirable, for example if a robust method could be formulated that includes the effect of loading style parameters. Alternatively, if the blade section geometry and aerodynamics are known, ΔT^* can be simply calculated from Eq. (15) and directly inputted into the correlation (Eq. (13)), removing almost all of the empiricism in the current method.

5.4 Open-Source Code

To facilitate comparison with future datasets, the correlation has been published as an open-source matlab code from the mathswork file exchange[1]. This code includes options to specify ΔT^* directly rather than using the correlation, and can perform simple design sweeps.

6. CONCLUSIONS

A new correlation for endwall loss has been developed, which synthesizes the surface dissipation approach of Denton [1] with the classical secondary flow theory of Hawthorne [23]. The method uses only low-order input parameters: flow angles at inlet and exit; velocity ratio; aspect ratio; pitch-to-axial-chord; platform lengths; blade maximum thickness and inlet boundary

[1] https://uk.mathworks.com/matlabcentral/fileexchange/180113-correlation-for-turbine-endwall-loss-coull-gt2025-151998

layer parameters. The correlation is formulated for linear cascades, but can predict realistic increases in endwall loss as we move from cascade-like to turbine-like inlet conditions, which have higher shape factor.

The correlation procedure can be summarized as follows:

1. The Wetted-Area-Loss is calculated by approximating the integral of velocity-cubed over the endwall surfaces and assuming a typical dissipation coefficient of 0.002.
2. The Secondary-Flow-Induced loss is calculated in stages:
   (a) The difference in transit time between flow passing over the pressure and suction sides is correlated. This sets the theoretical circulation of the passage vortex.
   (b) A first-order correction for streamtube contraction is applied to the inlet conditions.
   (c) The loss is calculated as the sum of (1) a term proportional to the circulation and (2) the Secondary Kinetic Energy term, from theory.

The correlation has been tuned using a large database of ~500 CFD calculations and blind validation has been performed with experimental cascade data from the literature. The new method has several advantages:

1. It is more accurate than existing methods. The average error in predicting experimental cascade loss was 30% lower than the next-best method.
2. The correlation is more physical than previous methods, directly representing the key mechanisms governing endwall loss.
3. At a high level, the empirical aspects of the correlation are minimal. Only 2 coefficients were optimized with the CFD database.
4. The correlation is the first to capture the effects of inlet boundary layer shape factor. Computations have previously shown that high shape factor can increase loss by a factor of 2 or more.

Further experimental data is needed to test the predictions of the new method, in particular to obtain data on the effect of inlet shape factor.

ACKNOWLEDGMENTS

Thanks are due to Rolls-Royce plc. for funding and permission to publish. Valuable comments are acknowledged from Andrew Melzer, Haidong Li, Tyler Gillen, Sarah Tooze and Raul Vasquez of Rolls-Royce, and Chris Clark of the University of Cambridge.

NOMENCLATURE

C_D	Dissipation Coefficient
CF	Contraction Factor (Eq. (21))
C_x	Axial Chord
h	Span
H_{12}	Inlet Boundary Layer Shape Factor
p	Pitch
$\dot{S}$	Entropy Generation Rate
ΔT^*	Non-Dimensional Transit Time Difference
T_{max}	Maximum Blade Thickness
V	Velocity
X_{DS}	Downstream Platform Length
X_{US}	Upstream Platform Length
α	Midspan Swirl Angle
γ	Ratio of Specific Heats
δ^*	Inlet Displacement Thickness
ρ	Density
Γ^*_{sec}	Non-Dimensional Passage Vortex Circulation ([14])
Π_{sec}	Vorticity Distribution Parameter ([14])
ζ	Kinetic Energy Loss Coefficient

Superscripts and Abbreviations

1	Inlet
2	Outlet
eff	Effective
end	Endwall
PS	Pressure Surface
sec	Secondary Flow
$sec-mix$	Secondary Flow Mixing
SS	Suction Surface
SKE	Secondary Kinetic Energy
wet	Wetted Area

REFERENCES

[1] Denton, J. "The 1993 IGTI Scholar Lecture: Loss Mechanisms in Turbomachines." *Journal of Turbomachinery* Vol. 115 No. 4 (1993): pp. 621–656. DOI 10.1115/1.2929299.

[2] Hawthorne, W.R. "Flow through Moving Cascades of Lifting Lines with Fluctuating Lift." *Journal of Mechanical Engineering Science* Vol. 15 No. 1 (1955): pp. 1–10. DOI 10.1243/jmes_jour_1973_015_003_02.

[3] Hodson, H.P. and Dominy, R. "Three-Dimensional Flow in a Low-Pressure Turbine Cascade at Its Design Condition." *Journal of Turbomachinery* Vol. 109 No. 2 (1987): pp. 177–185. DOI 10.1115/1.3262083.

[4] Hodson, H.P. and Dominy, R. "The Off-Design Performance of a Low Pressure Turbine Cascade." *Journal of Turbomachinery* Vol. 109 (1987): pp. 201–209. DOI 10.1115/1.3262086.

[5] Squire, H. and Winter, K. "The Secondary Flow in a Cascade of Airfoils in a Nonuniform Stream." *Journal of the Aeronautical Sciences* Vol. 18 No. 4 (1951): pp. 271–277. DOI 10.2514/8.1925.

[6] Coull, J.D. "Endwall loss in turbine cascades." *Journal of Turbomachinery* Vol. 139 No. 8 (2017): p. 081004. DOI 10.1115/1.4035663.

[7] Sieverding, C. "Recent Progress in the Understanding of Basic Aspects of Secondary Flows in Turbine Blade Passages." *Journal of Engineering for Gas Turbines and Power* Vol. 107 No. 2 (1985): pp. 248–257. DOI 10.1115/1.3239704.

[8] Langston, L. "Secondary Flows in Axial Turbines—A Review." *Annals of the New York Academy of Sciences* Vol. 934 No. 1 (2001): pp. 11–26. DOI 10.1111/j.1749-6632.2001.tb05839.x.

[9] Denton, J. and Pullan, G. "A Numerical Investigation Into the Sources of Endwall Loss in Axial Flow Turbines." *Amer-*

ican Society of Mechanical Engineers, Volume 8: Turbomachinery, Parts A, B, and C (2012)DOI 10.1115/gt2012-69173.

[10] Dunham, J. and Came, P. "Improvements to the Ainley-Mathieson Method of Turbine Performance Prediction." *Journal of Engineering for Power* Vol. 92 No. 3 (1970): pp. 252–256. DOI 10.1115/1.3445349.

[11] Craig, H. and Cox, H. "Performance Estimation of Axial Flow Turbines." *Proceedings of the Institution of Mechanical Engineers* Vol. 185 No. 1 (1971): pp. 407–424. DOI 10.1243/pime_proc_1970_185_048_02.

[12] Dunham, J. "A Review of Cascade Data on Secondary Losses in Turbines." *Journal of Mechanical Engineering Science* Vol. 12 No. 1 (1970): pp. 48–59. DOI 10.1243/jmes_jour_1970_012_009_02.

[13] Benner, M., Sjolander, S. and Moustapha, S. "An Empirical Prediction Method for Secondary Losses in Turbines: Part II — A New Secondary Loss Correlation." *Journal of Turbomachinery* Vol. 128 No. 2 (2006): pp. 281–291. DOI 10.1115/1.2162594.

[14] Coull, J.D. and Clark, C.J. "The Effect of Inlet Conditions on Turbine Endwall Loss." *Journal of Turbomachinery* Vol. 144 No. 10 (2022): p. 101011.

[15] Ainley, D. and Mathieson, G. "Performance of Axial-Flow Turbines." *Proceedings of the Institution of Mechanical Engineers* Vol. 159 No. 1 (1957): pp. 230–244. DOI 10.1243/pime_proc_1948_159_021_02.

[16] Kacker, S. and Okapuu, U. "A Mean Line Prediction Method for Axial Flow Turbine Efficiency." *Journal of Engineering for Power* Vol. 104 No. 1 (1982): pp. 111–119. DOI 10.1115/1.3227240.

[17] Traupel, W. "Thermal turbo-engines. Vol. I. Thermodynamic-fluidic calculation." *Springer-Verlag* (1977).

[18] Marsh, H. "Secondary Flow in Cascades: The Effect of Axial Velocity Ratio." *Journal of Mechanical Engineering Science* Vol. 16 No. 6 (1976): pp. 402–407. DOI 10.1243/jmes_jour_1974_016_074_02.

[19] Vazquez, R., Antoranz, A., Cadrecha, D. and Armananzas, L. "The Influence of Reynolds Number, Mach Number and Incidence Effects on Loss Production in Low Pressure Turbine Airfoils." *Turbo Expo: Power for Land, Sea, and Air*. 2006. DOI 10.1115/GT2006-91121.

[20] Coull, J.D., Clark, C.J. and Vazquez, R. "The sensitivity of turbine cascade endwall loss to inlet boundary layer thickness." *Journal of the Global Power and Propulsion Society* Vol. 3 (2019): pp. 540–554. DOI 10.22261/OEYMDE.

[21] Drela, M. and Giles, M. "Viscous-inviscid analysis of transonic and low Reynolds number airfoils." *4th Applied Aerodynamics Conference*, Vol. 25. 10: pp. 1347–1355. 1987. American Institute of Aeronautics and Astronautics. DOI 10.2514/6.1986-1786.

[22] Pullan, G., Denton, J.D. and Curtis, E. "Improving the performance of a turbine with low aspect ratio stators by aft-loading." *Journal of Turbomachinery* Vol. 128 No. 3 (2006): pp. 492–499. DOI 10.1115/1.2182000.

[23] Hawthorne, W.R. "Rotational flow through cascades Part I: the components of vorticity." *The Quarterly Journal of Mechanics and Applied Mathematics* Vol. 8 No. 3 (1955): pp. 266–279. DOI 10.1093/qjmam/8.3.266.

[24] Marsh, H. "Secondary Flow in Cascades: The Effect of Compressibility." *Aeronautical Research Council Reports and Memoranda* No. 3778 (1975).

[25] Benner, M., Sjolander, S. and Moustapha, S. "An Empirical Prediction Method for Secondary Losses in Turbines: Part I — A New Loss Breakdown Scheme and Penetration Depth Correlation." *Journal of Turbomachinery* Vol. 128 No. 2 (2006): pp. 273–280. DOI 10.1115/1.2162593.

[26] Coull, J.D., Clark, C.J. and Vazquez, R. "The sensitivity of turbine cascade endwall loss to inlet boundary layer thickness." *Journal of the Global Power and Propulsion Society* Vol. 3 (2019): p. OEYMDE. DOI 10.22261/jgpps.oeymde.

[27] Moinier, P. and Giles, M.B. "Preconditioned Euler and Navier-Stokes calculations on unstructured meshes." *6th ICFD Conference on Numerical Methods for Fluid Dynamics*. 1998.

[28] Menter, F. "Two-equation eddy-viscosity turbulence models for engineering applications." *AIAA Journal* Vol. 32 No. 8 (1994): pp. 1598–1605. DOI 10.2514/3.12149.

[29] Walsh, J.A. and Gregory-Smith, D.G. "Inlet skew and the growth of secondary losses and vorticity in a turbine cascade." *Journal of turbomachinery* Vol. 112 No. 4 (1990): pp. 633–642. DOI 10.1115/1.2927704.

[30] Sharma, O.P. and Butler, T.L. "Predictions of Endwall Losses and Secondary Flows in Axial Flow Turbine Cascades." *Journal of Turbomachinery* Vol. 109 No. 2 (1987): pp. 229–236. DOI 10.1115/1.3262089.

[31] Benner, M.W., Sjolander, S.A. and Moustapha, S.H. "Measurements of Secondary Flows Downstream of a Turbine Cascade at Off-Design Incidence." *Turbo Expo: Power for Land, Sea, and Air*: pp. 1299–1311. 2004. DOI 10.1115/GT2004-53786.

[32] Harrison, S. "Secondary Loss Generation in a Linear Cascade of High-Turning Turbine Blades." *Journal of Turbomachinery* Vol. 112 No. 4 (1990): pp. 618–624. DOI 10.1115/1.2927702.

[33] Brear, M., Hodson, H., Gonzalez, P. and Harvey, N. "Pressure Surface Separations in Low-Pressure Turbines—Part 2: Interactions With the Secondary Flow." *Journal of Turbomachinery* Vol. 124 No. 3 (2002): pp. 402–409. DOI 10.1115/1.1450765.

[34] de la Rosa Blanco, E., Hodson, H.P., Vazquez, R. and Torre, D. "Influence of the state of the inlet endwall boundary layer on the interaction between pressure surface separation and endwall flows." *Proceedings of the Institution of Mechanical Engineers, Part A: Journal of Power and Energy* Vol. 217 No. 4 (2003): pp. 433–441. DOI 10.1243/095765003322315496.

[35] Gregory-Smith, D., Graves, C. and Walsh, J. "Growth of Secondary Losses and Vorticity in an Axial Turbine Cascade." *Journal of Turbomachinery* Vol. 110 No. 1 (1988): pp. 1–8. DOI 10.1115/1.3262163.

[36] Folk, M., Miller, R.J. and Coull, J.D. "The impact of combustor turbulence on turbine loss mechanisms." *Journal of Turbomachinery* Vol. 142 No. 9 (2020): p. 091009. DOI 10.1115/1.4047615.

[37] Perdichizzi, A. *Mach Number Effects on Secondary Flow Development Downstream of a Turbine Cascade*. American Society of Mechanical Engineers (1990): pp. 643–651. DOI 10.1115/89-gt-67.

[38] Perdichizzi, A. and Dossena, V. "Incidence Angle and Pitch-Chord Effects on Secondary Flows Downstream of a Turbine Cascade." *ASME J. Turbomach* Vol. 115 (1993): pp. 383–391. DOI 10.1115/1.2929265.

[39] Weiss, A. and Fottner, L. "The Influence of Load Distribution on Secondary Flow in Straight Turbine Cascades." *Journal of Turbomachinery* Vol. 117 No. 1 (1995): pp. 133–141. DOI 10.1115/1.2835631.

[40] Yamamoto, A. "Production and Development of Secondary Flows and Losses in Two Types of Straight Turbine Cascades: Part 1—A Stator Case." *Journal of Turbomachinery* Vol. 109 No. 2 (1987): pp. 186–193. DOI 10.1115/1.3262084.

APPENDIX A. TRANSIT TIME DIFFERENCE

The transit time in equation (15) can be rewritten in terms of the suction and pressure surfaces contributions, including the surface lengths (S_0) and average inverse velocities:

$$\Delta T^* = T^*_{PS} - T^*_{SS} = \left(\frac{S_{0-PS}}{C_x}\right)\overline{\left(\frac{V_2}{V_{PS}}\right)} - \left(\frac{S_{0-SS}}{C_x}\right)\overline{\left(\frac{V_2}{V_{SS}}\right)} \quad (24)$$

The overbars indicate surface-length-averages. Table 3 shows the variation in these terms across the CFD database. Correlations are given in the table for three of the terms in Eq. (24), along with the accuracy of the fits. The remaining term, the inverse pressure surface velocity $\overline{(V_2/V_{PS})}$ is responsible for most of the variation in transit time and requires a more complex correlation. An aggregate of two methods are used to estimate this parameter; both of which consider the cross-passage pressure gradient due to turning inside the blade. Method 2 is usually more accurate, but tends to under-predict ΔT^* in some cases. Method 1 tends to over-predict these cases. The aggregate method therefore defaults to Method 2 except where there is a large discrepancy between the two methods, when it takes an average. Though relatively complex, this aggregate approach achieves reasonable accuracy and robustness.

Both methods follow the approach of Coull [14], and model the blade-to-blade geometry, Fig. 16(a), with an equivalent curved passage, Fig. 16(b). By considering free vortex flow through the equivalent curved passage, the pressure side velocity can be estimated.

A.1 Method 1

We first estimate the radius of curvature of the PS and then use the pitch and max thickness to calculate the SS curvature:

$$\frac{R_{PS}}{C_x} = \frac{1}{|\sin\alpha_1 - \sin\alpha_2|} \quad (25)$$

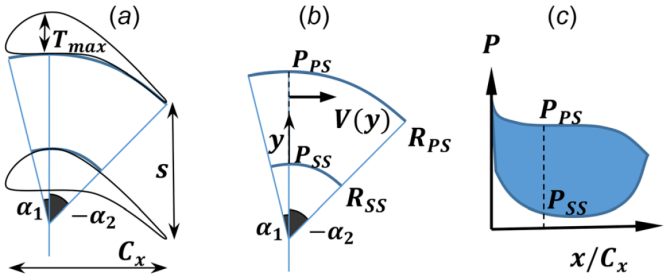

FIGURE 16: Free Vortex model to estimate the pressure surface velocity, [6].

$$\frac{R_{SS}}{C_x} = \frac{R_{PS}}{C_x} - \frac{(p - T_{max})}{C_x} \quad (26)$$

The average pressure side velocity, $\overline{(V_{PS}/V_2)}$, is correlated by:

$$\overline{\left(\frac{V_{PS}}{V_2}\right)} = \frac{\left(\frac{p}{R_{PS}}\right)}{0.352\left(\cos\alpha_2 + 1.864 max\left(\frac{R_{SS}}{R_{PS}}, -1.5\right) - 3.10\right)^2} \quad (27)$$

This parameter is clipped to be in the range 0.05-0.9. We then correlate for the average inverse $\overline{(V_2/V_{PS})}$. Note that because there is a distribution of velocity over the surface, this is not simply $\overline{(V_{PS}/V_2)}^{-1}$:

$$\overline{\left(\frac{V_2}{V_{PS}}\right)}_{Meth1} = 0.9641\overline{\left(\frac{V_{PS}}{V_2}\right)}^{-1} + 0.01974\overline{\left(\frac{V_{PS}}{V_2}\right)}^{-4.1106} \quad (28)$$

And thus ΔT^*_{Meth1} is calculated using Eq. (24).

A.2 Method 2

In this approach, we first estimate R_{SS} directly and then add the passage width to obtain R_{PS}:

$$\frac{R_{SS}}{C_x} = \frac{0.7}{|\sin\alpha_2|} \quad (29)$$

$$\frac{R_{PS}}{C_x} = \frac{R_{SS}}{C_x} + \frac{(p - T_{max})}{C_x} \quad (30)$$

TABLE 3: Terms in Transit Time Correlation, Eq. (24).

Term	Variation: Mean ± Std. Dev.	Correlation	Residual Error
$\left(\frac{S_{0-PS}}{C_x}\right)$	1.39 ±0.26	$\approx\frac{0.4267}{\cos\alpha_2} + 0.5086$	0.063 (1.6%)
$\overline{\left(\frac{V_2}{V_{PS}}\right)}$	3.25 ±2.17	See below	0.19 (5%)
$\left(\frac{S_{0-SS}}{C_x}\right)$	1.62 ±0.32	$\approx\frac{0.5024}{\cos\alpha_2} + 0.5202$	0.033 (0.8%)
$\overline{\left(\frac{V_2}{V_{SS}}\right)}$	0.98 ±0.07	≈0.98	0.07 (7%)

The average pressure side velocity $\overline{(V_{PS}/V_2)}$ is given by the analytical expression in Coull [6]:

$$\overline{\left(\frac{V_{PS}}{V_2}\right)} = \frac{p\cos\alpha_2}{R_{PS}\ln\left(R_{PS}/R_{SS}\right)} \tag{31}$$

Method 2 then correlates directly for the pressure side transit time, including the density ratio:

$$T^*_{PS-Meth2} = \left(\frac{S_{0-PS}}{C_x}\right)\overline{\left(\frac{V_2}{V_{ps}}\right)} \approx \frac{\rho_1}{\rho_2}\left(Y + 0.0226Y^{4.434}\right) \tag{32}$$

where

$$Y = \left[\frac{\left(1.075 - \frac{0.109}{\cos\alpha_2}\right)}{\overline{\left(\frac{V_{PS}}{V_2}\right)}}\right] \tag{33}$$

Again, ΔT^*_{Meth2} is calculated using Eq. (24):

$$\Delta T^*_{Meth2} = max\left[0, T^*_{PS-Meth2} - \left(\frac{S_{0-SS}}{C_x}\right)\overline{\left(\frac{V_2}{V_{ss}}\right)}\right] \tag{34}$$

A.3 Aggregate Method

The relative error between the methods is quantified as:

$$err = \frac{\left|\Delta T^*_{Meth2} - \Delta T^*_{Meth1}\right|}{\Delta T^*_{Meth2}} \tag{35}$$

A linear interpolation is used to switch between method 2 (for low error) and an average of methods 1 & 2 (for high error):

$$\Delta T^* = \begin{cases} \Delta T^*_{Meth2} & err < 0.29 \\ T^*_{Meth2} + \frac{\left(\Delta T^*_{12} - \Delta T^*_{Meth2}\right)(err - 0.29)}{0.02} & 0.29 \leqslant err \geqslant 0.31 \\ \Delta T^*_{12} & err > 0.31 \end{cases} \tag{36}$$

where

$$\Delta T^*_{12} = 0.5(\Delta T^*_{Meth1} + \Delta T^*_{Meth2}) \tag{37}$$

A sensible limiter of $\Delta T^* \leq 12$ is then applied. The accuracy of the different methods is shown in Fig. 2 in the main text. Method 2 achieves the lowest average fitting error, but the aggregate method has very similar accuracy and reduces the number of extreme outliers.

APPENDIX B. EXPERIMENTAL DATABASE

Table 4 list the key parameters of the experimental test cases.

TABLE 4: Key Parameters from Experimental Database.

Investigators	Cases	α_1 (°)	α_2 (°)	M_2	p/C_x	h/C_x	$\frac{Z_{TE}}{h}$, [25]	$\frac{\zeta_{profile}}{\zeta_{mid}}$, [25]	ζ_{end} (%) (Post-Correction)
Benner et al. [25], LS2	3	28.4 → 48.4	−53.6 → −49	0.1	0.738	1.36	0.15 → 0.24	0.76 → 0.85	3.42 → 4.76
Benner et al. [25], LS3	3	28.4 → 48.4	−52.6 → −47.3	0.1	0.741	1.36	0.15 → 0.23	0.77 → 0.85	2.58 → 6.29
Brear et al. [33]	4	30.4	−62.5 → −62.3	0.1	0.819	2.96	0.10	0.90	1.06 → 1.51
Folk et al. [36]	1	40	−65.5	0.14	1.04	1.35	0.226	0.774	2.72
Gregory-Smith et al. [35]	3	42.7 → 42.8	−67.5	0.1	1.09	2.61	0.18 → 0.28	0.72 → 0.82	3.41 → 4.38
Harrison [32]	4	40	−65.5	0.14	1.04	1.35	0.226	0.774	2.55 → 3.78
Hodson & Dominy [3]	1	38.8	−54.1	0.71	0.6	1.93	0.127	0.873	2.69
Hodson & Dominy [4]	8	18.5 → 47.4	−54.3 → −53.5	0.71	0.49 → 0.73	1.93	0.08 → 0.16	0.84 → 0.92	1.52 → 3.55
Perdichizzi [37]	6	17.4	−61.9	0.32 → 1.38	0.888	1.48	0.18 → 0.20	0.81 → 0.83	1.14 → 1.87
Perdichizzi & Dossena [38]	6	−16.1 → 13.9	−75 → −71.6	0.7	0.94 → 1.41	1.47	0.18 → 0.26	0.74 → 0.82	1.39 → 2.33
Weiss & Fottner [39], T104	1	37.7	−63.2	0.59	0.969	3.83	0.123	0.877	1.28
Weiss & Fottner [39], T106	1	37.7	−63.2	0.59	0.929	3.49	0.119	0.881	1.04
Yamomoto [40]	1	−2.9	−67.7	0.1	0.942	1.23	0.117	0.883	1.68
de la Rosa Blanco [34], thick	3	31.8	−63	0.1	0.96	2.96	0.12	0.88	1.15 → 1.61
de la Rosa Blanco [34], thin	3	31.8	−63	0.1	0.96	2.96	0.12	0.88	1.21 → 2.99